

Origin of Fine Structure of the Giant Dipole Resonance in sd -Shell Nuclei

R. W. Fearick,¹ B. Erler,² H. Matsubara,^{3,4} P. von Neumann-Cosel,² A. Richter,² R. Roth,² and A. Tamii³

¹*Department of Physics, University of Cape Town, Rondebosch 7700, South Africa*

²*Institut für Kernphysik, Technische Universität Darmstadt, D-64289 Darmstadt, Germany*

³*Research Center for Nuclear Physics, Osaka University, Ibaraki, Osaka 567-0047, Japan*

⁴*National Institute of Radiological Sciences, Chiba 263-8555, Japan*

(Dated: December 7, 2024)

A set of high resolution zero-degree inelastic proton scattering data on ^{24}Mg , ^{28}Si , ^{32}S , and ^{40}Ca provides new insight into the long-standing puzzle of the origin of fragmentation of the Giant Dipole Resonance (GDR) in sd -shell nuclei. Understanding is provided by state-of-the-art theoretical Random Phase Approximation (RPA) calculations for deformed nuclei using for the first time a realistic nucleon-nucleon interaction derived from the Argonne V18 potential with the unitary correlation operator method and supplemented by a phenomenological three-nucleon contact interaction. A wavelet analysis allows to extract significant scales both in the data and calculations characterizing the fine structure of the GDR. The fair agreement supports that the fine structure arises from ground-state deformation driven by α clustering.

PACS numbers: 24.30.Cz, 25.40.Ep, 21.60.Jz, 27.30.+t

Introduction. The isovector giant dipole resonance is the best known of the fundamental collective excitations of the nucleus [1]. A collective excitation or giant resonance can be understood macroscopically as a bulk nuclear vibration, and microscopically in terms of coherent particle-hole excitations. The gross properties of the GDR such as the centroid in energy of the excitations and the strength in terms of sum rules are well understood. Less well understood are, however, the details of decay processes of the resonance. Various contributions to the width of the giant resonances have been identified [1, 2]: direct decay out of the continuum leading to an escape width Γ^\uparrow , coupling to two-particle two-hole states ($2p2h$) and then to many-particle many-hole ($npmh$) states giving rise to a spreading width Γ^\downarrow , and fragmentation of the elementary $1p1h$ states that form the resonance called Landau damping ΔE . These processes contribute to the total width of the resonance and manifest experimentally by different structures of the resonance.

A fragmentation of the GDR in p - and sd -shell nuclei on the scale of several MeV is long-established and has been interpreted as configurational splitting [3]. Recently, it has been argued that the strength distribution of the GDR in ^{12}C and ^{16}O reveals information on the role of different α -cluster configurations [4]. However, the observation of finer structures of the GDR in light nuclei on the scale of several hundred keV remains a puzzle. In general, the physical origin of this kind of structure must be related to the existence of complex configurations, different time scales in decay processes, or the removal of the angular-momentum substate degeneracy due to deformation. Taking ^{28}Si as an example of an sd -shell nucleus, structure on the finest scales was observed in reaction cross sections [5] and identified with Ericson fluctuations [6]. These are essentially a manifestation of the spreading width.

Fine structure of the GDR has also been observed in heavy nuclei [7, 8] and in other giant resonances such as the isoscalar giant quadrupole resonance (GQR) [9, 10], the Gamow-Teller resonance [11], or the magnetic quadrupole resonance [12, 13]. Some progress has been made in the understanding of the fine structure by comparison between experiment and theoretical calculations of the distribution of resonance strength. In the case of the GQR it has been demonstrated that the fine structure has its origin in the coupling of the $1p1h$ excitations that constitute the resonance to low-lying surface vibrations [9, 10], a mechanism discussed in Ref. [14]. However, in a recent study of a lighter nucleus (^{40}Ca) it was shown that Landau damping plays a role in the formation of fine structure [15]. The importance of Landau damping was also demonstrated for the GDR in ^{208}Pb [8].

Here we turn attention to the GDR in light nuclei with equal proton and neutron numbers Z and N , respectively. In the sd shell these nuclei are deformed and a key driver of deformation is the underlying α -cluster structure [16]. Does this structural feature manifest itself in the fragmentation of the GDR? An answer to this question has become possible by the confluence of two advances: (i) The recent availability of high-resolution zero degree inelastic proton scattering data from a series of light nuclei [17] permits fine structure in the spectra to be resolved while providing a high degree of selectivity towards 1^- states, and (ii) the availability of microscopic calculations of the GDR strength using the random phase approximation (RPA) on top of a deformed ground state with a realistic nucleon-nucleon interaction. These calculations do not include coupling to the continuum or to more complex configurations but probe the effect of deformation on the fine structure of the GDR in sd -shell nuclei. As shown below, a detailed comparison yields good agreement with experiment, which leads us to the conclusion

that deformation plays a key role in the formation of fine structure in these *sd*-shell nuclei.

A central part of this work is a quantitative characterization of scales of fragmentation in the GDR region. Various measures have been proposed in the past, viz. averaging of spectra at various scales [5], Fourier analysis [18], correlation analysis [19], the entropy index method [20, 21], local scaling dimension [22, 23], and wavelet analysis [24]. We have chosen wavelet analysis as it offers a quantification of the energy scales of fine structures while resolving the strength of fine structures in both excitation energy and energy scale. Thus structures can be localized to the excitation energy region of the GDR. The wavelet analysis of the experimental data and corresponding theoretical strength distributions then permits us to make comparisons of the energy scales describing the structures among different nuclei and with theory. Given the complexity of nuclear behavior, such comparisons are necessarily of semi-quantitative nature. We do not expect, for example, that theoretical calculations can yet provide an exact description of the scales of structure, but might expect similar distributions of scales. Here we focus on the nuclei ^{24}Mg , ^{28}Si , ^{32}S and ^{40}Ca , which allows to compare prolate deformed (^{24}Mg , ^{32}S), oblate deformed (^{28}Si), and spherical ground states (^{40}Ca).

Experiment. Measurements of inelastic proton scattering at high resolution and at forward angles including 0° have only recently become feasible [17, 25]. Data were taken at RCNP, Osaka, Japan with the Grand Raiden magnetic spectrometer for 295 MeV proton beams. Dispersion-matching techniques were applied to achieve high energy-resolution of the order 20 to 30 keV full width at half maximum (FWHM) near zero degree angles [17]. Targets consisted of isotopically enriched thin foils with areal densities of a few mg/cm^2 . The spectrometer placed at 0° covers an angular acceptance of $\pm 2.5^\circ$. The spectra analyzed here correspond to a mean scattering angle of 0.4° , where the cross sections for excitation of 1^- states by relativistic Coulomb excitation dominate [26]. The momentum acceptance of the spectrometer permitted to cover a range of roughly 5–25 MeV in excitation energy. Spectra of the GDR between 14 and 24 MeV after subtraction of instrumental background are shown in the l.h.s. of Fig. 1. A considerable amount of fine structure is visible indeed.

Analysis. The wavelet analysis of the spectra is illustrated by the example of the $^{28}\text{Si}(p, p)$ data [Fig. 2(a)]. It proceeds via the calculation of a wavelet coefficient C from the measured cross sections $\sigma(E)$ (expressed in Counts/channel)

$$C_i(\delta E) \equiv C(\delta E, E_i) = \frac{1}{\sqrt{\delta E}} \int \sigma(E) \Psi^* \left(\frac{E_i - E}{\delta E} \right) dE, \quad (1)$$

where E_i is the excitation energy of channel i , δE the wavelet scale, and Ψ the wavelet function. Here, the

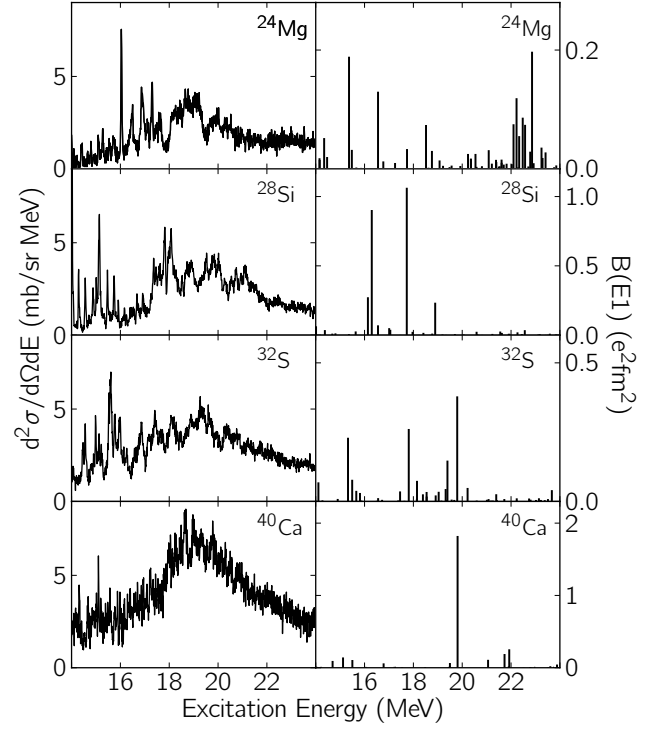


FIG. 1. Left: High-resolution (20 – 30 keV FWHM) spectra of the (p, p) reaction with $E_0 = 295$ MeV and $\theta_{lab} = 0.4^\circ$ for ^{24}Mg , ^{28}Si , ^{32}S , and ^{40}Ca . The excitation energy range shown encompasses the GDR. Right: Theoretical $B(E1)$ strengths calculated in a deformed-basis RPA with the UCOM interaction [16].

complex Morlet wavelet

$$\Psi(x) = \pi^{-1/4} e^{ik_0 x} e^{-x^2/2}, \quad (2)$$

with $k_0 = 5$ is employed, which provides optimum balance between resolution of excitation energy and energy scale. The wavelet decomposition is performed over the whole spectrum with reflective boundary conditions and a region of interest corresponding to the bulk of the GDR strength. The squares of the wavelet coefficients, representing a measure of the strength of structures resolved by the wavelets, are displayed in Fig. 2(b). Because of possible contributions to the spectra from spin- $M1$ excitations at lower excitation energies [27, 28], further analysis is restricted to the highlighted area (16 – 24 MeV). The projected power spectrum

$$P_w(\delta E) = \frac{1}{N} \sum_{i=i_1}^{i_2} |C_i(\delta E) C_i^*(\delta E)|, \quad (3)$$

where i_1 and i_2 indicate the boundaries of the region of interest, is shown in the lower left hand panel (c). Peaks of strength in this power spectrum are associated with characteristic scales of the structures in the region of the GDR. The power spectrum is normalized to the spectral

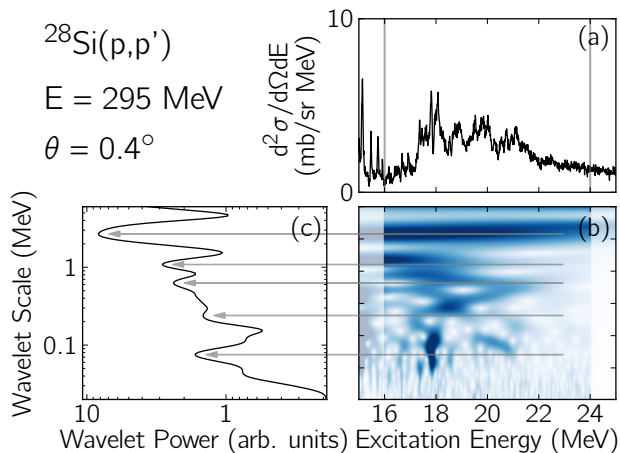


FIG. 2. Example of the wavelet analysis. (a) Experimental spectrum of the GDR in ^{28}Si from the (p, p) reaction. (b) Square of the wavelet coefficient C [Eq. (1)] as a function of E_x and wavelet scale. The highlighted area (16 – 24 MeV) is selected for projection onto the scale axis. (c) Wavelet power spectrum. The peaks quantitatively characterize the fine structure.

variance in order to facilitate comparison between different nuclei and with theoretical results.

For the case of ^{28}Si there are several sets of high resolution data available in the literature besides the (p, p) results (a) shown in the l.h.s. of Fig. 3: (b) the $^{28}\text{Si}(e, e')$ reaction [29, 30], (c) the $^{27}\text{Al}(p, \gamma)$ reaction [5], and (d) the $^{27}\text{Al}(p, \alpha_0)$ reaction [31, 32]. It is expected that reactions (a)-(c) predominantly excite the GDR. Reaction (d) favors isospin $T = 0$ states in ^{28}Si and is therefore not selective towards 1^- levels but may provide a possible window into more general origins of fine structure. These data were analyzed in the same way and the resulting wavelet coefficient plots are displayed on the r.h.s. of Fig. 3. Not only can corresponding structures be located in the experimental spectra, but also in the wavelet plots there is a good agreement between the two-dimensional distributions of wavelet power demonstrating the utility and reliability of the wavelet method. The striking similarities of the results underline that the structures extracted with the wavelet analysis are indeed intrinsic features of the nuclei involved.

RPA calculations. For comparison with the experimental measurements, theoretical $B(E1)$ strength distributions were calculated in the random phase approximation (RPA) starting from axially deformed Hartree-Fock (HF) ground states and using explicit angular-momentum projection techniques. Both the HF and the RPA calculations use the same realistic nucleon-nucleon interaction derived from the Argonne V18 potential by a unitary transformation in the framework of the Unitary Correlation Operator Method (UCOM) [33, 34] and are supplemented by a phenomenological three-nucleon contact

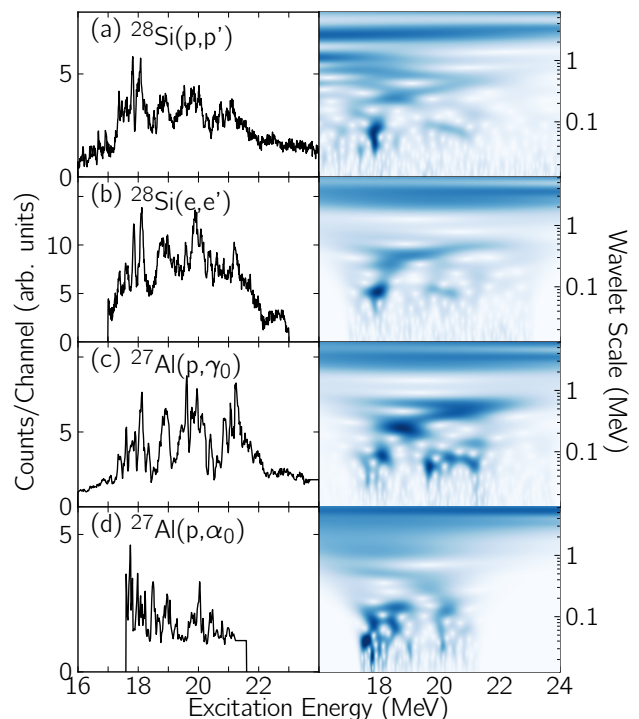


FIG. 3. Left: Experimental data from different high-resolution experiments populating the GDR in ^{28}Si . Right: Wavelet analysis.

interaction. This Hamiltonian was introduced and tested in Ref. [35] for ground-state observables and applied for RPA calculations in closed-shell nuclei in Ref. [36] (we use the version labeled ‘S-UCOM(SRG)’). All calculations are performed in a harmonic-oscillator single-particle basis covering 15 oscillator shells. Further details on the deformed RPA approach employed in this work can be found in Ref. [16].

The resulting theoretical strengths are shown in the right column of Fig. 1. The distribution of positions (as a rough measure of the widths) and relative strengths reproduce the data fairly well without the inclusion of complex configurations through a second-RPA formulation which was required for the GQR [10]. The calculation does not include the continuum and so the strength distribution consists of discrete transitions. For the subsequent wavelet analysis a Gaussian with a width determined by the experimental resolution was folded into the distributions so that the low-scale cutoff in the wavelet power spectra matched the experimental data.

These RPA strength distributions were also analyzed with the wavelet method. The power spectra from this analysis (Fig. 4) reproduce features of the experimental data like the common observation of a scale around 100 keV and a typical number of 3 – 4 scales between 100 keV and 1 MeV. However the overall rise of power at larger scales in the data is not observed. To some extent

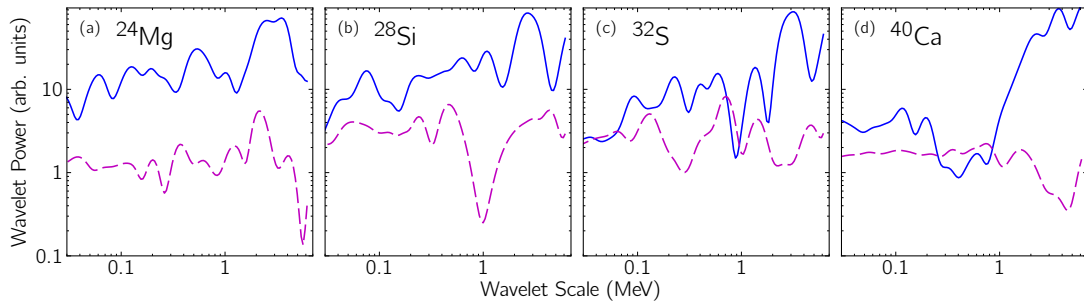


FIG. 4. Wavelet power spectra of the GDR in ^{24}Mg , ^{28}Si , ^{32}S , and ^{40}Ca from the data of Fig. 1. Blue solid lines: experiment. Dashed magenta lines: theory.

this is due to the ability of the wavelet analysis to resolve features both in spacing and in shape. The Morlet wavelet yields local wavelength information because of its oscillatory shape but it also functions as a generalized second derivative operator giving an enhanced signal for the broad bell-shaped distribution of GDR strength in the experimental spectra. Thus large scales with high strength observed in the experimental data are not replicated in the theoretical analysis because the continuum is not included in the calculations. Convolution of the theoretical strengths with a Lorentzian curve of suitable width broadens the lines and indeed enhances the large-scale wavelet power but is artificial in the absence of knowledge of the true widths. We thus choose to analyze the theoretical results as is.

Discussion. The analysis reveals a considerable degree of fine structure in the deformed nuclei in the sd shell, while it is relatively weak in the closed shell nucleus ^{40}Ca . Table I summarizes the significant scales in ^{28}Si in the wavelet power spectra for all experimental data and theoretical calculations. These can be grouped in three classes: in all the experimental spectra there is a scale (Class I) at approximately 80 keV. This is similar to the average level width due to Ericson fluctuations in ^{28}Si [5] and we tentatively follow this identification. It conforms with the absence of a corresponding scale in the theoretical results. At larger energies scales similar in energy

to those in $^{28}\text{Si}(p, p')$ are seen in the $^{28}\text{Si}(e, e')$ data and in the $^{27}\text{Al}(p, \gamma)$ data; the $^{27}\text{Al}(p, \alpha)$ data shows similar numbers of scales but with slightly shifted energy. These are denoted Class II and Class III, where Class III scales are large scales associated with the spread of the distribution of strength while Class II are intermediate scales in the region 100 keV to about 1 MeV. Similar results are obtained for the other nuclei chosen for study, ^{24}Mg , ^{32}S and ^{40}Ca as illustrated in Fig. 4 although in the case of ^{40}Ca the Class II scales are rather weak and the power spectrum is dominated by Class III. Comparable scales to those seen in the analysis of the experimental data are found also in the theoretical strength, not only in Class III, representing the spread in strength, but also in Class II. Thus already at the RPA level in our realistic calculations there is considerable fragmentation of the strength, and the scales and number of scales of strength are similar in both experiment and theory. The origin of this fragmentation in the theoretical spectrum is the deformation of the nucleus driven by the strong α clustering in these nuclei [16]. This suggests that a prime source of the fine structure in the GDR in light nuclei is deformation rather than the coupling to surface vibrations invoked for the GQR in heavier nuclei [9, 10]. This observation is supported by the case of the closed shell nucleus ^{40}Ca where both experiment and theory exhibit only weak fine structures of Class I and II.

Finally we illustrate an additional utility of the wavelet method. The calculations do not clearly prefer oblate over prolate deformation for the ground state of ^{28}Si [16]. However, the scale spectra are rather different and allow us to pick out the oblate deformation as more readily matching the experimental data. The corresponding wavelet analysis is shown in Fig. 5.

Conclusions. We have available, for the first time, a set of high resolution data for the GDR region of $N = Z$ nuclei in the sd shell, together with RPA calculations performed on top of a deformed ground state with a realistic nucleon-nucleon interaction. This enables us to address the long-standing question of the origin of fine structure of the GDR in nuclei in this mass region. A wavelet analysis permits us to extract scales characterizing this fine

TABLE I. Characteristic scales of the fine structure of the GDR in ^{28}Si from different experiments and theoretical RPA results assuming an oblate (o) or prolate (p) ground state. Scales are divided in three classes (see text).

Spectrum	Scales (MeV)		
	Class I	Class II	Class III
$^{28}\text{Si}(p, p')$	0.075	0.23, 0.36, 0.59	1.0, 2.9
$^{28}\text{Si}(e, e')$	0.084	0.23, 0.36	1.0, 3.3
$^{27}\text{Al}(p, \gamma)$	0.076	0.14, 0.24, 0.38, 0.59	1.1, 3.2
$^{27}\text{Al}(p, \alpha)$	0.092	0.12, 0.40	0.9, 2.6
^{28}Si RPA (o)		0.23, 0.44	2.1
^{28}Si RPA (p)		0.18 0.80	1.6

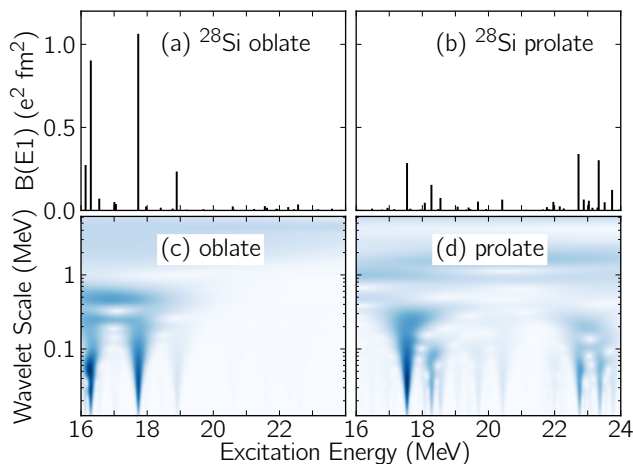


FIG. 5. Theoretical $B(E1)$ strength distributions and their wavelet analysis for the case of an oblate (a,c) or a prolate (b,d) ground state deformation of ^{28}Si .

structure and the results for different reactions leading to the GDR in ^{28}Si shows that good consistency is achieved. Comparisons between experimental data and the RPA calculations indicate that the fine structure arises from the deformation of the nucleus driven by α clustering. This is in sharp contrast to the case of the GQR in heavier nuclei where coupling to $2p2h$ states is the driver.

We acknowledge support by the DFG under contracts SFB 634 and NE 679/3-1, by the BMBF under contracts 06DA9040I and 06DA7047I, and by the South African NRF.

[1] M. N. Harakeh and A. van der Woude, *Giant Resonances: Fundamental High-Frequency Modes of Nuclear Excitation*, (Oxford University Press, Oxford, 2001).
[2] P. F. Bortignon, A. Bracco, and R. A. Broglia, *Giant Resonances: Nuclear Structure at Finite Temperature* (Harwood Academic, Amsterdam, 1998).
[3] R. A. Eramzhayan *et al.*, Phys. Rep. **136**, 229 (1986).
[4] W. B. He *et al.*, Phys. Rev. Lett. **113**, 032506 (2014).

[5] P. Singh *et al.*, Nucl. Phys. **65**, 577 (1965).
[6] T. Ericson, Phys. Rev. Lett. **5**, 430 (1960).
[7] C. Iwamoto *et al.*, Phys. Rev. Lett. **108**, 262501 (2012).
[8] I. Poltoratska *et al.*, Phys. Rev. C **89**, 054322 (2014).
[9] A. Shevchenko *et al.*, Phys. Rev. Lett. **93**, 122501 (2004).
[10] A. Shevchenko *et al.*, Phys. Rev. C **79**, 044305 (2009).
[11] Y. Kalmykov *et al.*, Phys. Rev. Lett. **96** (2006) 012502.
[12] P. von Neumann-Cosel *et al.*, Phys. Rev. Lett. **82**, 1105 (1999).
[13] Y. Kalmykov *et al.*, Phys. Rev. Lett. **99**, 202502 (2007).
[14] G. F. Bertsch, P. F. Bortignon, and R. A. Broglia, Rev. Mod. Phys. **55**, 287 (1983).
[15] I. Usman *et al.*, Phys. Lett. B **698**, 191 (2011).
[16] B. Erler and R. Roth, submitted to Phys. Rev. C; arXiv:1409.0826 [nucl-th].
[17] A. Tamii *et al.*, Nucl. Instrum. Methods A **605**, 3 (2009).
[18] A. Richter, in *Nuclear Spectroscopy and Reactions, Part B*, edited by J. Cerny (Academic Press, New York, 1974) p. 343.
[19] G. Kilgus *et al.*, Z. Phys A **326**, 41 (1987).
[20] D. Lacroix and P. Chomaz, Phys. Rev. C **60**, 064307 (1999).
[21] D. Lacroix *et al.*, Phys. Lett. B **479**, 15 (2000).
[22] H. Aiba and M. Matsuo, Phys. Rev. C **60**, 034307 (1999).
[23] H. Aiba *et al.*, Phys. Rev. C **83**, 024314 (2011).
[24] A. Shevchenko *et al.*, Phys. Rev. C **77**, 024302 (2008).
[25] R. Neveling *et al.*, Nucl. Instrum. Methods A **654**, 29 (2011).
[26] C. A. Bertulani and G. Baur, Phys. Rep. **163**, 299 (1988).
[27] K. Heyde, P. von Neumann-Cosel, and A. Richter, Rev. Mod. Phys. **82**, 2365 (2010).
[28] H. Matsubara, PhD thesis, University of Osaka (2010); and to be published.
[29] A. Friebel, Doctoral thesis D17, Technische Hochschule Darmstadt (1981).
[30] A. Richter, Prog. Part. Nucl. Phys. **13**, 1 (1985).
[31] G. P. Lawrence and A. R. Quinton, Nucl. Phys. **65**, 275 (1965).
[32] L. W. Put, J. D. A. Roeders, and A. Van der Woude, Nucl. Phys. **A112**, 561 (1968).
[33] H. Feldmeier *et al.*, Nucl. Phys. **A632**, 61 (1998).
[34] R. Roth, T. Neff, and H. Feldmeier, Prog. Part. Nucl. Phys. **65**, 50 (2010).
[35] A. Günther *et al.*, Phys. Rev. C **82**, 024319 (2010).
[36] A. Günther, P. Papakonstantinou, and R. Roth, arXiv:1303.6098 [nucl-th].